Valley caloritronics and its realization by graphene nanoribbons

Xiaobin Chen,[1,*] Lei Zhang,[1,2] and Hong Guo[1]

[1]*Department of Physics, Center for the Physics of Materials, McGill University, Montreal, Quebec H3A 2T8, Canada*

[2]*State Key Laboratory of Quantum Optics and Quantum Optics Devices, Institute of Laser Spectroscopy, Shanxi University, Taiyuan 030006, China*

(Received 11 June 2015; revised manuscript received 18 September 2015; published 21 October 2015)

We propose and theoretically investigate an idea of valley caloritronics where quantum transport of the *valley* degrees of freedom is thermally induced. Valley caloritronics addresses questions such as thermal generation of valley polarized current and, more importantly, pure valley current without an accompanying charge current. After establishing a general physical picture, we show that heat-induced pure valley current can be generated by virtue of wedge-shaped graphene nanoribbons in a two-probe device setup. We discover that the quantum transport properties of the valley degree of freedom can be very different when driven by a voltage bias or by a temperature bias. A very surprising result is that an alternating valley current can be *thermally* generated via gate control: namely the heat-induced valley current changes its flow direction in some quasiperiodic manner versus the value of a gate voltage at a fixed polarity. Our results indicate a vast potential for developing valley caloritronic devices.

DOI: 10.1103/PhysRevB.92.155427 PACS number(s): 73.63.−b, 72.80.Vp, 73.23.Ad, 74.78.Na

I. INTRODUCTION

Accompanying the world's ever-increasing demand for energy, there is, in fact, a huge energy loss in the form of waste heat [1]. Harvesting waste heat for useful purposes is now a central theme of energy research and various thermal devices such as thermal insulators, junctions, diodes, and memories have been hotly pursued [2–5]. Thermoelectric effects, which are on the boundaries of phononics and electronics, could be very advantageous for turning waste heat into useful energy [6,7]. Waste heat is not only commonplace in industrial processes and consumer products, it is also a major problem in computer technology, where the power density has reached such a high level as to threaten the stability of integrated circuits. To possibly remedy the latter problem, new ideas for logic devices beyond the principles of present-day field effect transistor (FET) are being heavily investigated in both communities of science and engineering, with the focus on systems that require much less energy to operate than FETs. For instance, using the fact that the energetic scale of spin dynamics is several orders of magnitudes smaller than that required for charge dynamics, logic devices based on spintronics are very interesting for energy-efficient information processing, where the information carrier is no longer the charge states but spin states [8].

The most recent advance along this line of thought is the low-dissipation *valleytronic* devices that can be designed for storing, extracting, and manipulating bits of information encoded in the valley quantum index. In semiconductors, a valley means a local energy extremum in the Brillouin zone (BZ). In valleytronics, the information carrier is thus the valley degree of freedom of the electrons, and the excitement is the idea of using discrete values of the crystal momentum for quantum information. The generation of valley polarization has been experimentally realized in several material systems, including the $SiO_2/Si(100)/SiO_2$ quantum wells [9], AlAs two-dimensional electron gas [10], bismuth [11], diamond [12], $MoSe_2$ [13], and monolayer MoS_2 [14–16]. In addition, there have been several observations and theoretical predictions for valley-polarized currents using optical excitation in MoS_2 [17] and WSe_2 [18–20]. In 2D crystals with Fermi-pocket anisotropy, it was anticipated that both valley current and spin current could be acquired [21]. In carbon systems, it was proposed that 100% valley filters could be realized in nanojunctions such as wedge-shaped graphene nanoribbons (GNRs) [22], carbon nanotube and GNR junctions [23], as well as graphene sheet with grain boundaries [24,25]. As a charge-neutral current, a pure valley current manifests itself in nonlocal voltage measurements [26], and may play an important role in future valleytronic devices [27]. Theoretically, pure valley current is proposed to be generated by quantum pumping in graphene under strain and electric field barrier as well as a ferromagnetic field [28], by adjusting ferromagnetic exchange field and local external electric field in a normal-ferromagnetic-normal silicene junction [29], or by utilizing second-order nonlinear responses to bias and temperature gradient in 2D materials [21].

So far, most valleytronics systems were based on electrical or optical properties of materials. In this paper, we propose and investigate an idea where quantum transport of the valley degree of freedom is thermally induced, and we shall call this line of research in the general area of valley caloritronics (VCT). VCT addresses the question of how to directly use thermal means to generate a valley polarized current and more importantly, pure valley current without an accompanying charge current. Such a heat-induced valley current is fundamentally interesting and also offers a different control of the valley degree of freedom. Generally speaking, we envision VCT to focus on the interplay of heat and valley currents, a spirit that is reminiscent to the spin caloritronics [30–32]. Finally, we envision VCT to devote to understanding thermoelectric transport effects in materials where nonequilibrium valley populations occur. The purpose of this work is to report a first investigation of basic issues to the notion of VCT, namely heat-induced valley polarized currents and pure valley currents.

*xbchen@physics.mcgill.ca

In particular, we show that heat-induced valley currents are simple to manipulate and have a strong output due to the first-order response nature of the transport physics. Our analysis reveals that heat-induced valley polarized charge currents and even pure valley currents—without an accompanying charge current—can be produced by virtue of a valley filter in the traditional two-probe device setup. In addition, we discover that an alternating valley current can be *thermally* generated via gate control: a very surprising result is that the heat-induced valley current changes its flow direction in some quasiperiodic manner versus the value of a gate voltage having a fixed polarity. In Sec. II, a general physical picture of heat-induced valley current is established and relevant theoretical formulation presented. In Sec. III, we show that the general physical picture can be realized by a graphene valley filter and we present the numerical results to demonstrate the properties of heat-induced valley quantum transport. Finally, Sec. IV is reserved for a summary.

II. GENERIC PHYSICS OF VALLEY CALORITRONICS

We start by a theoretical discussion of quantum transport in a generic system having a valley degree of freedom. Without losing generality, let's assume there are two well-separated valleys labeled by the valley quantum index $\eta = 1,2$, and the valley-resolved transmission function is $\Xi^\eta(E)$. For a given voltage bias ΔV or temperature bias ΔT, the valley-resolved charge current J_η, the total charge current J_c, and the total valley current J_v are obtained from the following formula within the Landauer quantum transport picture:

$$J_\eta = \frac{-2e}{h}\int (f_L - f_R)\Xi^\eta(E)dE, \quad (\eta = 1,2), \tag{1}$$

$$J_c = J_1 + J_2, \tag{2}$$

$$J_v = J_1 - J_2, \tag{3}$$

respectively. Here, h is the Planck's constant, $e(>0)$ is the value of elementary charge, and f_L (f_R) is the Fermi-Dirac distribution function of the left (L) (or R) lead. In linear response, i.e., when $\Delta V \to 0$, $\Delta T \to 0$, by Taylor expansion the valley-resolved charge current J_η is reduced to

$$J_\eta = G_\eta \Delta V + G_\eta S_\eta \Delta T, \quad \eta = 1,2, \tag{4}$$

where G_η is the valley-resolved conductance and S_η the valley-resolved Seebeck coefficient, and it is not difficult to derive [33,34]

$$G_\eta = \frac{2e^2}{h}\int \Xi^\eta(E)(-\partial_E f)|_{T,\mu}dE, \tag{5}$$

$$S_\eta = -\frac{1}{eT}\frac{\int \Xi^\eta(E)(E-\mu)(\partial_E f)|_{T,\mu}dE}{\int \Xi^\eta(E)(\partial_E f)|_{T,\mu}dE}. \tag{6}$$

Equation (4) shows that a valley-selective conductance naturally results in a valley-selective electric current under a voltage bias and/or a temperature bias. Therefore, thermally induced electric currents in valley-filtering configurations are generally valley-polarized.

Based on this simple formulation, let's discuss the possibility of generating a *pure* valley current J_η—without an accompanying charge current J_c—by thermal means. Physically, a pure valley current may be interpreted as a flow that only transport *lattice momenta*. Theoretically, according to Eqs. (2) and (3) this should be possible when $J_1 = -J_2$ so that $J_c = 0$ and $J_v \neq 0$. In other words, a *pure* valley current is possible if valley-1 and valley-2 currents have the same amplitude but move in opposite direction [Fig. 1(a)]. Clearly, such a flow pattern is impossible to establish in a two-probe device if there is only a voltage bias ΔV, since by Eq. (4) $J_\eta = G_\eta \Delta V$ and the conductances G_η are positive numbers. This situation is schematically shown in Fig. 1(b) where J_1 and J_2 flow in the same direction, thus $J_c \neq 0$, so one could obtain a valley-polarized current but not a pure valley current.

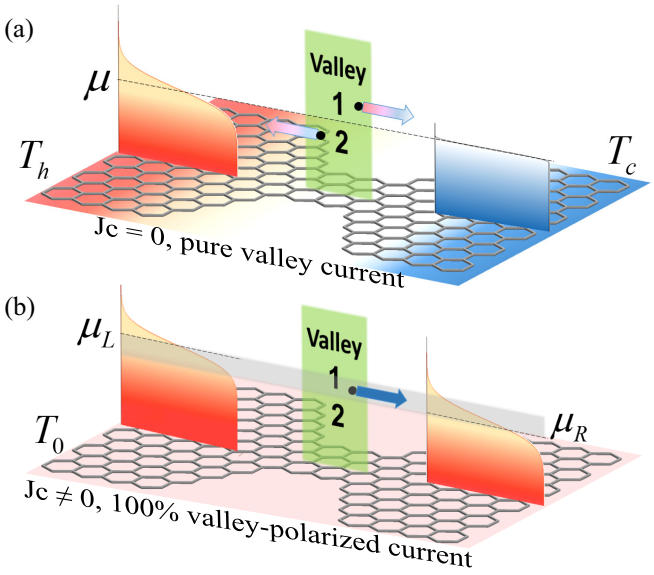

FIG. 1. (Color online) Illustration of the difference between thermally driven and electrically driven valley-resolved currents. (a) Under a temperature bias, electrons of different valleys move in opposite directions if their Seebeck voltages ΔV_T^η have different signs. (b) Under a voltage bias, electrons within the energy window $[\mu_R, \mu_L]$ of both valley 1 and valley 2 move in the same direction.

However, a thermal bias makes it feasible to induce a pure valley current. Assuming $\Delta V = 0$, $\Delta T \neq 0$, and introduce a quantity called "valley Seebeck voltage" $\Delta V_T^\eta \equiv S_\eta \Delta T$, then by Eq. (4) we obtain $J_\eta = G_\eta \Delta V_T^\eta$. Note that S_η can have both positive and negative signs [see Eq. (6)], thus the valley Seebeck voltage ΔV_T^η could in principle be positive for valley 1 but negative for valley 2, resulting to the flow pattern in Fig. 1(a). When $G_1 S_1 = -G_2 S_2$, we have J_1 canceling J_2, which means a pure valley current is obtained.

Physically, with a voltage bias electrons are driven by ∇V to flow in the same direction regardless of their valley index [Fig. 1(b)], hence there is always a nonzero charge current J_c. On the other hand, with a temperature bias electrons are driven by the *valley Seebeck voltage* ΔV_T^η, which allows electrons having different valley quantum index to move in different directions [Fig. 1(a)], and this could lead to a pure valley current J_η with a zero accompanying charge current J_c. We conclude that both voltage bias and temperature bias can generate fully valley-polarized charge currents, but only the latter can achieve the flow of pure valley currents.

III. VALLEY CALORITRONICS BY GRAPHENE NANORIBBONS

Having established the theoretical formulation and qualitative physical picture of valley caloritronics, in this section we investigate a material system that can realize VCT. To this end we consider GNRs, which have several advantages. First, graphene typically has high thermal stability as suggested by its high melting temperature of 4510 K [35]. Second, due to a large separation of the two valleys in graphene or GNRs, little effect from electron-phonon coupling is expected between the valleys [36]. Third, wedge-shaped GNRs were predicted to act as 100% valley filters [22], hence their application to realize VCT should be effective. Finally, carbon nanojunctions are homojunctions and their integration into an all-carbon circuit in the future is quite natural.

Figure 2(a) shows the two-probe structure of a wedge-shaped 12-4-12 zigzag GNR (ZGNR) junction, where the numbers indicate how many lines of carbon in the left lead, central region, and right lead, respectively. The corresponding band structures of the ZGNRs are shown in Fig. 2(b), where the single transport mode around the Fermi energy of the narrow ribbon [right-hand side of Fig. 2(b)] is clearly depicted. Also indicated, different modes from the source of the two-probe device [left-hand side of Fig. 2(b)] have the same energy but different wave vectors $\boldsymbol{k}$, resulting in different transmission probabilities: the modes with $\boldsymbol{k}$ matching that of the central region is expected to have higher transmission [22].

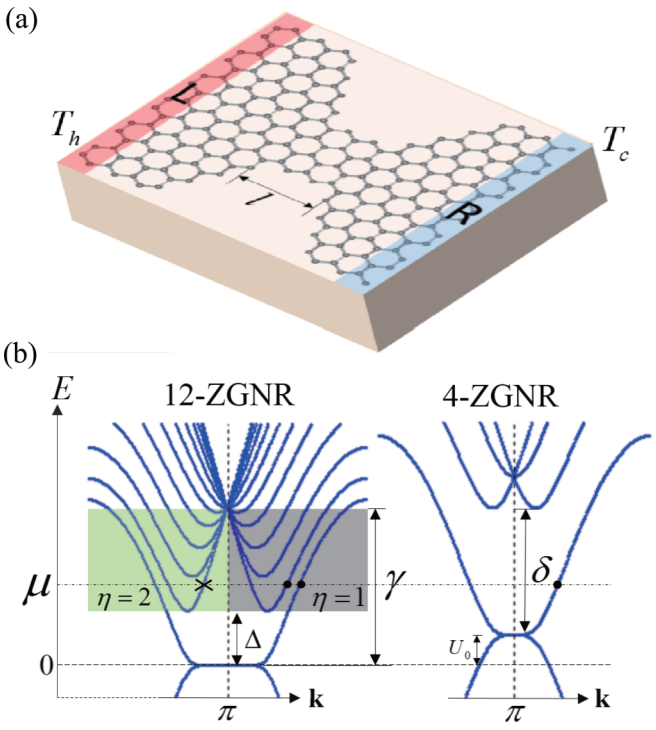

FIG. 2. (Color online) (a) Schematic plot of a valley filter consisting of a wedge-shaped GNR connected to two ideal semi-infinite N-ZGNR leads, where N is the number of zigzag lines of carbon atoms. l labels the length of the central constricted region. This figure is thus a 12-4-12 wedge-shaped GNR junction. A temperature gradient across the device is established by the hot and cold temperatures, T_h, T_c. (b) Band structures of a N-ZGNR lead and the central constricted region. The shaded area is valley degenerated and can be divided into channels belonging to the two valleys labeled by $\eta = 1,2$. U_0 is the gate voltage applied on the central region of length l.

For numerical calculation of the theoretical expressions in Sec. II, we use a single-band tight-binding (TB) Hamiltonian [22],

$$H = \gamma \sum_{\langle i,j \rangle} c_i^\dagger c_j + \sum_i U_i c_i^\dagger c_i, \tag{7}$$

where the on-site energy of p_z orbital is zero, the nearest-neighbor hopping integral $\gamma = -2.6$ eV, and U_i is the applied gate voltage at the ith site. In this paper, the central restriction region of length l is applied with a gate voltage of $U_i = U_0$. Although ground state of a ZGNR is antiferromagnetic [37], it is reported that a ZGNR could be spin-polarized or spin-unpolarized under different bias voltages [38], and it becomes nonmagnetic when concentration of edge defects reaches 0.1/Å [39]. Previous works also showed that edge defects had no significant effect on the operation of valley filters [22]. Therefore, in this work we consider edge regular nonmagnetic structures and the on-site Coulomb repulsion [32] can be neglected when illustrating the VCT idea. The two-probe device can be considered as consisting of three parts: the left and right leads, which are perfect ZGNRs,[1] and the central scattering region [Fig. 2(a)].

Using a mode-matching numerical approach [22,40,41], the total transmission coefficient can be written as a summation over individual transport channels as

$$\Xi(E) = \sum_{\eta=1,2} \Xi^\eta(E), \ \Xi^\eta(E) = \sum_n \Xi_n^\eta(E), \tag{8}$$

where $\Xi_n^\eta(E)$ is the partial transmission of electrons with energy E at the nth mode and valley η coming from lead L to lead R, and $\Xi^\eta(E)$ is the valley-resolved transmission function. Accordingly, the valley polarization of the total transmission is defined as

$$P(E) = \frac{\Xi^1(E) - \Xi^2(E)}{\Xi^1(E) + \Xi^2(E)}. \tag{9}$$

Before moving forward, we note that transport properties of wedge-shaped GNRs have been previously explored in the literature [22,42,43] and we have verified the valley-filtering effect by investigating a 12-4-12 wedge-shaped GNR, and these details are included in the Appendix. It turns out that $n_1/n_2/n_1$ wedge-shaped ZGNRs with even numbers of n_1, n_2, which are central-symmetric structures, have better valley-filtering effects. This might be closely related to symmetries of wave functions [44,45].

In the following, from the calculated transmission functions we apply Eqs. (1)–(3) to determine valley-resolved charge currents J_η as well as total charge current J_c and valley current J_v. We investigate a 140-40-140 wedge-shaped ZGNR with $l = 34a$, $a = 2.46$ Å. In this system, the minimum energies of the second subband closest to $|E| = 0$ of the lead GNR and

[1]For armchair GNRs, the valley degree of freedom quench due to the folding of the BZ.

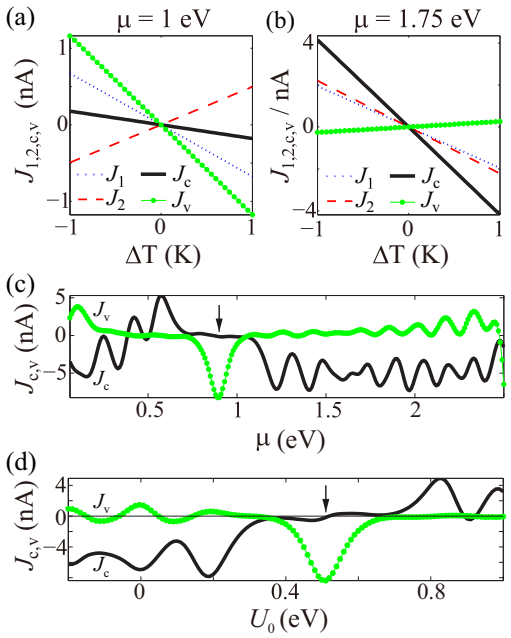

FIG. 3. (Color online) Thermally driven charge (thick black), valley 1 (blue dotted), valley 2 (red dash), and valley (green line dotted) currents of a gated 140-40-140 wedge-shaped and $l = 34a$ ZGNR as a function of temperature difference, $\Delta T = T_L - T_R$ with $T_R = 300$ K, and (a) $\mu = 1$ eV, (b) $\mu = 1.75$ eV. The gate voltage is set to be $U_0 = 0.9$ eV. Also, the charge current and the valley current as a function of (c) the system's chemical potential, μ, with $U_0 = 0.9$ eV, $\Delta T = 1$ K, and of (d) the gate voltage, U_0, with $\mu = 0.5$ eV. Arrows in (c) and (d) mark points of pure valley currents.

central GNR are $\Delta \approx 0.09$ eV and $\delta \approx 0.30$ eV, respectively. As drawn in Fig. 3(a), the currents are of the order of nA under a ΔT of about 1 K and change linearly versus ΔT. Valley-polarized currents of this scale is experimentally detectable.

Figure 3(a) also shows a good linearity of thermoelectric currents to ΔT. The linearity guarantees linear controllability of valley currents and is expected to maintain well within the feasible temperature differences, because the characteristic thermal energy $k_B \Delta T$ is only about 0.025 eV even when $\Delta T =$ 300 K, where k_B is the Boltzmann constant.

When $\mu_L = \mu_R \equiv \mu = 1$ eV, $U_0 = 0.9$ eV, and $\Delta T > 0$ [Fig. 3(a)], we find $J_1 < 0$ and $J_2 > 0$, which indicate a concomitant "electron-like" and "hole-like" transport, respectively. Here, both the charge current J_c and valley current J_v are in the same direction with J_1 because $|J_1| > |J_2|$. However, when the chemical potential of the system is varied, magnitudes and signs of the valley currents also vary as shown in Fig. 3(b). The direction change of valley-resolved currents originates from the sign change in S_η; i.e., the sign change of the valley Seebeck voltage as discussed in Sec. II. Therefore, the direction and magnitude of $J_{1,2}$ and thus J_v can be finely tuned by the sign and value of the temperature difference, by the chemical potential and by the gate voltage, because Seebeck coefficients depend on these factors.

To determine the tuning effects of chemical potential, we plot J_c and J_v as a function of μ in Fig. 3(c): J_c and J_v are quite out-of-phase and both have various magnitudes and directions as a function of μ. They do not share every zero points and there are several μ values where $J_v \neq 0$ but $J_c = 0$, meaning a pure-valley current is flowing inside the device. In particular, one can find such a point around U_0 ($\mu \approx 0.86$ eV). The gate voltage dependence of J_c and J_v is shown in Fig. 3(d), and there is a significant variation in valley current—changing both magnitude and direction, as a function of the gate voltage. Thus, a pure valley current is generated at a proper gate voltage such as $U_0 \approx 0.52$ eV. We conclude that pure valley currents can be generated by tuning the chemical potential and/or gate voltage under a temperature gradient.

In Fig. 4(a), thermally driven currents at the pure-valley-current point found in Fig. 3(d), are drawn explicitly. It clearly shows that currents from different valleys have different directions and the same magnitude, resulting in charge-neutral current and nonzero pure valley current. The linearity of pure valley current to ΔT is maintained very well. The corresponding valley-resolved Seebeck coefficients are plotted in Fig. 4(b) and indeed, they have different signs and reflect the variation of valley-resolved conductance [see Fig. 4(c)] as implied by the Mott's Relation [33], $S_\eta \approx -(\pi^2 k_B^2 T/3e)[\ln G_\eta(E)]'|_{E=\mu}$. From these results, we observe $\mu = U_0$ being a special point: valley 1 dominates the conduction when $\mu > U_0$, while valley 2 does so when $\mu < U_0$. If the filtered transmission keeps strict symmetry about $\mu = U_0$, then $G_1 = G_2$, $S_1 = -S_2$, and pure valley current can be expected at this symmetric point. For wedge-shaped graphene, note that the point for a pure valley current in Fig. 4(a) is close but not exactly at $\mu = U_0$: due to the asymmetry of transmission from the lead L to the conduction bands and valence bands of the narrow region in the device structure. Normally, a pure valley current can be expected around an intersection of $G_1(E)$ and $G_2(E)$, as the case shown in Fig. 4(c). In this case, transmission polarization changes its sign on the cross point. However, in regions where one valley dominates, e.g., $G_1 > G_2$, there are also possible points where pure valley currents can be achieved, as long as the variation of G_2 is different to and larger than that of G_1 such that $|S_1| < |S_2|$, making $G_1 S_1 + G_2 S_2 = 0$ possible.

In addition to the valley-polarized and pure valley current, it is very interesting to point out that an "alternating" valley

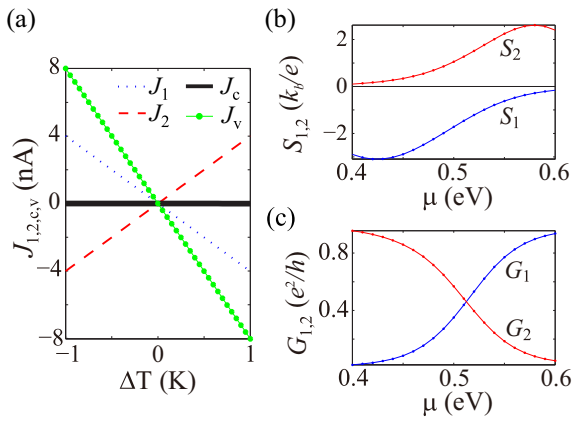

FIG. 4. (Color online) Realization of pure valley current. (a) The pure valley current at $\mu = 0.5$ eV, $U_0 = 0.522$ eV for the marked point in Fig. 3(d). The corresponding valley-resolved (b) Seebeck coefficients, $S_{1,2}$, and (c) conductance, $G_{1,2}$, for valley-1 and valley-2 electrons.

current can be realized versus gate voltage. As depicted in Fig. 3(d), J_v changes its sign as U_0 varies, for example, when $0 < U_0 < 0.2$ eV. Importantly, the sign of J_v is changed in an alternating fashion without changing the *sign* of U_0, which means a true alternating valley current is induced by simply tuning the magnitude of gate voltage but not its polarity. Again, the physical origin of this effect is due to the sign change of the valley Seebeck voltage when U_0 is varied.

Finally, a discussion on experimental realization of our idea is in order. The size constriction in the GNR device structure plays an important role. A sufficient condition for acquiring pure valley current around $\mu = U_0$ is that transporting channels belong to different valleys when channel energies are above or below U_0. This condition is guaranteed by the valley-filtering effect of the single-valley bands in the central constricted region of the device structure. Combining the facts that electrons around $\mu \pm k_B T$ are relevant and that the single-valley constricted region should have bands in the energy window $[E_F - \delta, E_F + \delta]$ (E_F is the Fermi level of the corresponding ideal GNR), we deduce that $\delta \geqslant k_B T$ should be satisfied. Given that $\delta = 2|\gamma|\cos[(N-1)\pi/(2N+1)] \approx 3\pi|\gamma|/2N$ when $N \gg 1$ and that $T = 300$ K [42], we estimate $N_{\max} \approx 490$ with a width of about 100 nm. Thus, the central region of a wedge-shaped GNR is expected to function well at room temperature when the central constricted width is not wider than 100 nm. GNRs at such a scale can nowadays be routinely achieved in nanofabrication facilities. So far we have used edge regular nonmagnetic structures to demonstrate the notion of valley caloritronics. This assumption is, however, unnecessary, namely if the central region is in the antiferromagnetic ground state, which generates an energy gap to hinder thermal activation of charge carriers and thus the realization of pure valley current, an extra transverse electric field can be applied to close the energy gap of one spin channel [37,46] and pure valley current can be robustly generated.

IV. CONCLUSIONS

In conclusion, we have carried out a first investigation to the notion of valley caloritronics. Our general theoretical analysis shows that valley-polarized currents can be generally generated in a valley-filtering configuration, and that valley currents driven by voltage bias and by temperature bias can produce very different quantum transport of the valley degree of freedom. In particular, a pure valley current—without an accompanying charge current—can be induced if there is a temperature bias. The general physical picture can be realized using the valley-filtering effect of wedge-shaped GNRs for which we predict highly valley-polarized and/or pure valley current can be induced by a temperature bias and controlled by a gate voltage. Here, ΔT drives charges in each valley to flow while the gate voltage tunes the particle energy to induce a pure valley current where the operating point is around $\mu = U_0$, i.e., when the central valley separation boundary aligns with the chemical potential. Remarkably, the valley current can reverse its flow direction as the value—but not the sign—of the gate voltage is tuned, hence an alternating valley current is obtained by the caloritronic system.

Since the physical picture is general, the VCT effects predicted in this work are anticipated in any system having a well-established valley degree of freedom. Many such materials exist, including Si, two-dimensional transition metal dichalcogenides and others. To achieve the pure valley current in these systems, one can also use a gate voltage or line defect to first establish a valley filter effect or to tune the valley-resolved Seebeck coefficients. Our results allow us to conclude that both valley-polarized charge current and pure valley current in nanostructures can be effectively manipulated by thermal means, paving the way to a large class of VCT systems.

ACKNOWLEDGMENTS

We gratefully acknowledge financial support by Natural Sciences and Engineering Research Council of Canada (NSERC) (H.G.). X.C. thanks China Scholarship Council and MESRS Merit Scholarship Program for Foreign Students 2014–2015. We thank Calcul Québec and Compute Canada for the computation facilities.

APPENDIX: VALLEY-FILTERING EFFECTS OF WEDGE-SHAPED GNRS

In this Appendix, we present transport properties of a wedge-shaped 12-4-12 ZGNR junction with a step-gate voltage $U_i = U_0$ applied across the narrow ribbon region and $l = 10a$. This analysis shows the valley filtering effects of this system.

Normally, longer restriction region in the center guarantees better filtering. In this case, $L = 10a$ is good enough to have a satisfactory valley filtering property. As shown in Fig. 5(a), transmission near $E = 0$ is rather small, consistent with previous findings that wedge-shaped ribbons have nonconducting localized states and a transmission gap near the Fermi energy [43]. Generally, the transmission function features spiky lines,

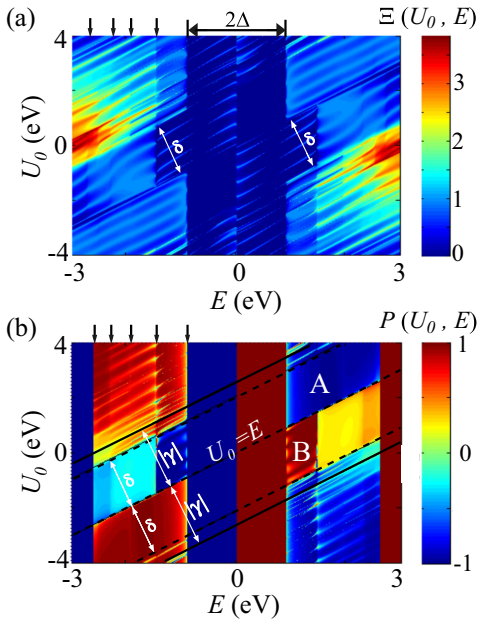

FIG. 5. (Color online) (a) Total transmission and (b) valley polarization of a gated wedge-shaped 12-4-12 ZGNR with the central restriction length $L = 10a$ as functions of gate voltage U_0 and energy E. Upper left black arrows in (b) indicate positions of band edges of the leads.

which are signs of resonant tunneling and are more distinct in small-sized junctions. In addition, the reversal symmetry of the transmission function, $\Xi(-U_0, -E) = \Xi(U_0, E)$, is clearly shown in the figure. The reversal symmetry can be attributed to the electron-hole symmetry of the graphene system. It is also interesting to observe in the figure that there are vertical boundaries, which actually correspond to band edges of the leads, and two oblique regions separated by $U_0 = E \pm \delta$ and $U_0 = E$, which are the single-valley band regions of the narrow ribbon. The filtering effect of the single-valley band can be seen more clearly in the polarization plot.

In Fig. 5(b), the valley polarization function is similarly plotted versus electron energy and gate voltage. For $|E| < \Delta$, within which accompanies vanishing transmission [42], valley polarization is strictly 1 or -1. The reason lies in the fact that electrons in the source belong to one valley as illustrated in Fig. 2(b), hence no actual filtering. For $E > \Delta$ and U_0 in $(E, E + \delta)$ [indicated as A region in Fig. 5(b)], where the single-valley band in the narrow region filters out valley-2 electrons coming from the left lead, polarization is close to -1 in spite of the rapid variation in transmission function. When U_0 is within $(E - \delta, E)$ [B region in Fig. 5(b)], polarization is opposite to that in A region and shows ripples, which are associated with resonant peaks shown in Fig. 5(a). Vertical boundaries in the plot are standing out and have the same positions as those in the transmission plot. Those boundaries indicate abrupt changes in the valley polarization which is expected to be $1/(2n + 1)$ when there are $2n + 1$ channels conducting in the central region [22]. Using a small-sized junction, we show in Fig. 5 the excellent filtering effect within the single-valley window of the narrow GNR region.

[1] A. Shakouri, Ann. Rev. Mater. Res. **41**, 399 (2011).
[2] B. Li, L. Wang, and G. Casati, Phys. Rev. Lett. **93**, 184301 (2004).
[3] L. Wang and B. Li, Phys. Rev. Lett. **101**, 267203 (2008).
[4] Y. Xu, X. Chen, J.-S. Wang, B.-L. Gu, and W. Duan, Phys. Rev. B **81**, 195425 (2010).
[5] N. Li, J. Ren, L. Wang, G. Zhang, P. Hänggi, and B. Li, Rev. Mod. Phys. **84**, 1045 (2012).
[6] D. Parker and D. J. Singh, Phys. Rev. X **1**, 021005 (2011).
[7] S. Wang, Z. Wang, W. Setyawan, N. Mingo, and S. Curtarolo, Phys. Rev. X **1**, 021012 (2011).
[8] S. A. Wolf, D. D. Awschalom, R. A. Buhrman, J. M. Daughton, S. von Molnár, M. L. Roukes, A. Y. Chtchelkanova, and D. M. Treger, Science **294**, 1488 (2001).
[9] K. Takashina, Y. Ono, A. Fujiwara, Y. Takahashi, and Y. Hirayama, Phys. Rev. Lett. **96**, 236801 (2006).
[10] O. Gunawan, Y. P. Shkolnikov, K. Vakili, T. Gokmen, E. P. De Poortere, and M. Shayegan, Phys. Rev. Lett. **97**, 186404 (2006).
[11] Z. Zhu, A. Collaudin, B. Fauque, W. Kang, and K. Behnia, Nat. Phys. **8**, 89 (2012).
[12] J. Isberg, M. Gabrysch, J. Hammersberg, S. Majdi, K. K. Kovi, and D. J. Twitchen, Nat. Mater. **12**, 760 (2013).
[13] Y. Li, J. Ludwig, T. Low, A. Chernikov, X. Cui, G. Arefe, Y. D. Kim, A. M. van der Zande, A. Rigosi, H. M. Hill, S. H. Kim, J. Hone, Z. Li, D. Smirnov, and T. F. Heinz, Phys. Rev. Lett. **113**, 266804 (2014).
[14] W. Yao, D. Xiao, and Q. Niu, Phys. Rev. B **77**, 235406 (2008).
[15] H. Zeng, J. Dai, W. Yao, D. Xiao, and X. Cui, Nat. Nanotechnol. **7**, 490 (2012).
[16] T. Cao, G. Wang, W. Han, H. Ye, C. Zhu, J. Shi, Q. Niu, P. Tan, E. Wang, B. Liu, and J. Feng, Nat. Commun. **3**, 887 (2012).
[17] K. F. Mak, K. L. McGill, J. Park, and P. L. McEuen, Science **344**, 1489 (2014).
[18] Y. J. Zhang, T. Oka, R. Suzuki, J. T. Ye, and Y. Iwasa, Science **344**, 725 (2014).
[19] H. Yuan, X. Wang, B. Lian, H. Zhang, X. Fang, B. Shen, G. Xu, Y. Xu, S.-C. Zhang, H. Y. Hwang, and Y. Cui, Nat. Nanotechnol. **9**, 851 (2014).
[20] L. Zhang, K. Gong, J. Chen, L. Liu, Y. Zhu, D. Xiao, and H. Guo, Phys. Rev. B **90**, 195428 (2014).
[21] H. Yu, Y. Wu, G.-B. Liu, X. Xu, and W. Yao, Phys. Rev. Lett. **113**, 156603 (2014).
[22] A. Rycerz, J. Tworzydło, and C. Beenakker, Nat. Phys. **3**, 172 (2007).
[23] H. Santos, L. Chico, and L. Brey, Phys. Rev. Lett. **103**, 086801 (2009).
[24] D. Gunlycke and C. T. White, Phys. Rev. Lett. **106**, 136806 (2011).
[25] D. Gunlycke, S. Vasudevan, and C. T. White, Nano Lett. **13**, 259 (2012).
[26] R. Gorbachev, J. Song, G. Yu, A. Kretinin, F. Withers, Y. Cao, A. Mishchenko, I. Grigorieva, K. Novoselov, and L. Levitov, Science **346**, 448 (2014).
[27] W.-Y. Shan, J. Zhou, and D. Xiao, Phys. Rev. B **91**, 035402 (2015).
[28] J. Wang, K. S. Chan, and Z. Lin, Appl. Phys. Lett. **104**, 013105 (2014).
[29] Z. P. Niu and S. Dong, Appl. Phys. Lett. **104**, 202401 (2014).
[30] G. E. W. Bauer, E. Saitoh, and B. J. van Wees, Nat. Mater. **11**, 391 (2012).
[31] M. Zeng, L. Shen, H. Su, c. Zhang, and Y. Feng, Appl. Phys. Lett. **98**, 092110 (2011).
[32] X. Chen, Y. Liu, B.-L. Gu, W. Duan, and F. Liu, Phys. Rev. B **90**, 121403 (2014).
[33] M. Cutler and N. F. Mott, Phys. Rev. **181**, 1336 (1969).
[34] X. Chen, D. Liu, W. Duan, and H. Guo, Phys. Rev. B **87**, 085427 (2013).
[35] J. H. Los, K. V. Zakharchenko, M. I. Katsnelson, and A. Fasolino, Phys. Rev. B **91**, 045415 (2015).
[36] D. Xiao, G.-B. Liu, W. Feng, X. Xu, and W. Yao, Phys. Rev. Lett. **108**, 196802 (2012).
[37] Y.-W. Son, M. L. Cohen, and S. G. Louie, Nature **444**, 347 (2006).
[38] D. Gunlycke, D. A. Areshkin, J. Li, J. W. Mintmire, and C. T. White, Nano Lett. **7**, 3608 (2007).
[39] B. Huang, F. Liu, J. Wu, B.-L. Gu, and W. Duan, Phys. Rev. B **77**, 153411 (2008).

[40] P. A. Khomyakov, G. Brocks, V. Karpan, M. Zwierzycki, and P. J. Kelly, Phys. Rev. B **72**, 035450 (2005).
[41] I. Rungger and S. Sanvito, Phys. Rev. B **78**, 035407 (2008).
[42] K. Wakabayashi, Phys. Rev. B **64**, 125428 (2001).
[43] F. Muñoz-Rojas, D. Jacob, J. Fernández-Rossier, and J. J. Palacios, Phys. Rev. B **74**, 195417 (2006).
[44] Z. Li, H. Qian, J. Wu, B.-L. Gu, and W. Duan, Phys. Rev. Lett. **100**, 206802 (2008).
[45] A. R. Akhmerov, J. H. Bardarson, A. Rycerz, and C. W. J. Beenakker, Phys. Rev. B **77**, 205416 (2008).
[46] J. Guo, D. Gunlycke, and C. T. White, Appl. Phys. Lett. **92**, 163109 (2008).